

FULL PAPER

Topology of planar corner-sharing network in B₂O₃ glass at intermediate range

Haruto Morimoto¹, Daiki Sugihara¹, Koji Kimura^{1,2,†}, Yohei Onodera², Qiao Xvsheng³, Jens R. Stellhorn⁴, Tomokatsu Hayakawa⁵, Shinji Kohara² and Koichi Hayashi¹

¹Department of Physical Science and Engineering, Nagoya Institute of Technology, Gokisocho, Showaku, Nagoya 466–8555, Japan

²Center for Basic Research on Materials, National Institute for Materials Science (NIMS), 1–2–1 Sengen, Tsukuba, Ibaraki 305–0047, Japan

³State Key Laboratory of Silicon and Advanced Semiconductor Materials & School of Materials Science and Engineering, Zhejiang University, Hangzhou 310058, China

⁴Co-Creation Institute for Advanced Materials, Shimane University, 1060 Nishi-Kawatsu-cho, Matsue 690–8504, Japan

⁵Department of Life Science and Applied Chemistry, Nagoya Institute of Technology, Gokisocho, Showaku, Nagoya 466–8555, Japan

B₂O₃ glass is a non-tetrahedral network-forming glass whose structure consists of boroxol rings that cannot form in crystalline phases under ambient conditions. In this study, a three-dimensional structural model of B₂O₃ glass containing a large fraction of boroxol rings (~80 %) was successfully constructed by reverse Monte Carlo (RMC) modeling on the basis of high-energy X-ray diffraction data. This achievement is notable given that maintaining such a large fraction of boroxol rings has traditionally been considered difficult in conventional RMC modeling. Analyses of coordination number, bond angle distributions, and ring size distribution confirmed that the boroxol rings were well preserved in the model. The ring size distribution and persistence diagram revealed that B₂O₃ glass contains a large fraction of boroxol rings and a small fraction of larger rings with exceptionally high topological order, compared with typical tetrahedral network-forming glasses such as SiO₂ glass. Our modeling and topological analysis can be extended to various B₂O₃-based glasses to provide a firm basis for understanding their physicochemical and structural properties at the atomic level.

Key-words : Topology, Reverse Monte Carlo, High-energy X-ray diffraction, B₂O₃ glass

[Received November 11, 2025; Accepted February 6, 2026; Published online March 19, 2026]

1. Introduction

B₂O₃ is one of the representative glass formers. Unlike other typical glass-forming oxides such as SiO₂ and P₂O₅, which are characterized by networks of tetrahedral structural units (SiO₄ or PO₄ tetrahedra), B₂O₃ glass is composed of triangular BO₃ structural units. Furthermore, a significant fraction of B atoms in B₂O₃ glass (hereafter denoted as *f*) is incorporated into a larger structural unit, the B₃O₆ boroxol ring.¹⁾ The value of *f* has been estimated to be 70–85 % using various techniques, such as nuclear magnetic resonance,^{2–4)} nuclear quadrupole resonance,⁵⁾ X-ray diffraction (XRD),⁶⁾ and neutron diffraction measurements.⁷⁾

To date, numerous studies have been performed to construct a structural model of B₂O₃ glass.^{8–20)} Such a model is crucial for understanding the origin of the physicochemical properties, including the boron anomaly in

alkali borate glasses,^{13,22,23)} superior chemical durability of borosilicate glasses,²⁴⁾ various optical properties of rare-earth-doped borate glasses,^{24–26)} and low melting and glass-transition temperatures of pure B₂O₃ glasses.^{27,28)} The reverse Monte Carlo (RMC) method²⁹⁾ is a powerful tool for constructing three-dimensional atomic configurations of glasses based on X-ray and neutron diffraction data. RMC calculations have been applied to B₂O₃ glass.^{18–21)} Although the structural models obtained in these studies successfully reproduced the experimentally obtained structure factors, the large fraction of B atoms incorporated into boroxol rings could not be accounted for in Refs. 18) and 21). In Refs. 19) and 20), the *f* value was not discussed in detail. Molecular dynamics (MD) simulations have also been extensively carried out.^{8–17)} Whereas in the early days, the formation of boroxol rings was not well reproduced by MD simulations,⁸⁾ reasonably large values of *f* have been obtained in more recent studies mainly because of the refinement of the interatomic potentials.^{12,14)} Despite these advances, reproducing such a boroxol-ring-rich network remains difficult within standard MD simulation procedures starting from random configurations. Moreover, diffraction data derived from the

[†] Corresponding author: K. Kimura; E-mail: kimura.koji@nitech.ac.jp

[‡] Preface for this article: DOI <https://doi.org/10.2109/jcersj2.134.P4-1>

MD-based structural models tend to show only moderate agreement with experimental results, particularly in the low-wavenumber (Q) region, when compared with RMC modelings. For example, Urata and Lodesani have recently reported the results of a combination of classical and ab initio MD simulations,¹⁷⁾ in which they controlled the fraction of boroxol rings in the initial configurations. In their study, the agreement of simulation data with diffraction data is insufficient, particularly for the principal peak (PP) observed at $Q \sim 3 \text{ \AA}^{-1}$ in the XRD data. As a result, reconciling diffraction data with a high f value has been considered challenging.

In addition to the techniques in the above studies, empirical potential structure refinement (EPSR)³⁰⁾ was also employed to build a structural model of B₂O₃ glass.³¹⁾ The X-ray- and neutron-weighted structure factors derived from the constructed structural model were in good agreement with experimental data with a maintaining large f value of $\sim 75\%$. The key idea in Ref. 31) was the incorporation of dummy atoms at the centers of boroxol rings to reinforce constraints and prevent their collapse during the structural refinement. This idea can also be applied to the RMC method. Although Swenson and Börjesson¹⁸⁾ concluded that it was not possible to construct a structural model with $f > 30\%$ using the RMC method based on neutron diffraction data, the concept of using dummy atoms could improve the RMC modeling for B₂O₃ glass.

In our previous studies, we have applied the RMC modeling technique to various glass systems,^{32–34)} and in the present work, we aim to extend this method to address the long-standing issue of boroxol ring fractions in B₂O₃ glass. In this work, we perform RMC modeling based on high-energy XRD data of B₂O₃ glass using a dummy-atom approach and successfully construct a structural model that reconciles the diffraction data with a large fraction of boroxol rings. The validity of the obtained structural model is confirmed in terms of the boroxol-ring fraction, diffraction data, coordination number, and bond-angle distribution. Furthermore, the ring size distributions, persistence diagrams, and cavity-volume analyses are applied to the constructed model, revealing an exceptionally high degree of topological order in B₂O₃ glass.

2. Experiment and modeling

The B₂O₃ glass was prepared by melting HBO₂ at 1300 °C in air for 90 min and quenching the melt in a brass mold. The glass samples were sealed in a vacuum-packed plastic bag to prevent moisture adsorption.

The high-energy XRD experiments were performed at BL04B2 in SPring-8.³⁵⁾ To measure high- Q diffraction data, XRD data were obtained at an incident energy of 61.3 keV. The scattering angle 2θ ranged from 0.300 to 48.9° using a combination of four CdTe and three Ge detectors. The corresponding Q ranged from 0.16 to 25.72 \AA^{-1} . The measurements took approximately 1.5 h.

A structural model of B₂O₃ glass was constructed by RMC modeling based on the XRD data using the RMC++ code.³⁶⁾ The initial atomic configuration was constructed

by dividing the oxygen atoms into two types, O⁽¹⁾ and O⁽²⁾. The O⁽¹⁾ and O⁽²⁾ atoms are defined by whether they were incorporated into the boroxol ring. The dummy atoms X were placed at the centers of the boroxol rings to reinforce the constraints for maintaining the shapes of the boroxol rings during the simulation. Here, the weighting factor of the dummy atoms for X-rays was set to 0. The length of the side of the simulation box was set to 33.45 \AA to reproduce the number density (0.0800 \AA^{-3}) of the sample.

The initial atomic configuration in RMC modeling is often obtained by MD simulations.^{32,33)} However, constructing the initial atomic configuration of B₂O₃ glass obtained by MD simulation is challenging because the boroxol rings easily collapse during the calculation in conventional RMC modeling. Therefore, the initial atomic configuration in this study was constructed as follows.

First, 400 boroxol rings consisting of three B atoms and three O⁽¹⁾ atoms were randomly distributed in the simulation box, taking into account reasonable distances between the rings. Next, the dummy X atoms were placed at the center of the 320 boroxol rings, whereas no dummy atoms were placed in the remaining 80 boroxol rings to deform their rings during the subsequent simulations. Hereafter, 240 O atoms belonging to the 80 boroxol rings without X atoms were treated as O⁽²⁾ atoms. Then, 600 O⁽²⁾ additional atoms were placed between two B atoms belonging to two different boroxol rings. The initial atomic configuration, which contains 3320 particles (1200 B, 1800 O, and 320 X atoms), was created by a hard-sphere Monte Carlo (HSMC) simulation. Two types of constraint were applied to avoid physically unrealistic structures: the closest atom–atom distance and the coordination number. The closest atom–atom distances for B–B, B–O, O–O, B–X, O–X, and X–X pairs were set to 2.10, 1.25, 2.10, 1.25, 1.25, and 1.00 \AA , respectively, to avoid unreasonable spikes in the partial pair distribution functions. The constraints on the B–O, O–B, X–B, and X–O coordination numbers were applied; all of the B atoms were coordinated to three O atoms, all of the O atoms were coordinated to two B atoms, and all of the X atoms were coordinated to three B and three O atoms. Furthermore, the constraints for B–X–B and O–X–O bond angles at 120° were applied. The first coordination distances for constraints for coordination numbers and bond angles were set to 1.5 \AA . The obtained initial atomic configuration is shown in Fig. 1. In addition to the boroxol rings bridged by the O⁽²⁾ atoms, BO₃ trigonal planars appear as a consequence of the collapse of the boroxol rings in the absence of X atoms at the center. After the HSMC simulation, the configuration was refined by RMC simulation with the constraints of the B–O, O–B, X–B, and X–O coordination numbers, and the B–X–B and O–X–O bond angles.

The bond angle distribution $B(\theta)$ was calculated as the number of bonds between $\theta + \Delta\theta$, which depends on the solid angle $\Delta\Omega \propto \sin(\theta)$ subtended at that value of θ . Each bond angle distribution was therefore plotted as $B(\theta)/\sin(\theta)$ to compensate for the effect of $\Delta\Omega$. The (B–O)_{*n*} ring size distribution of B₂O₃ glass was calculated from the

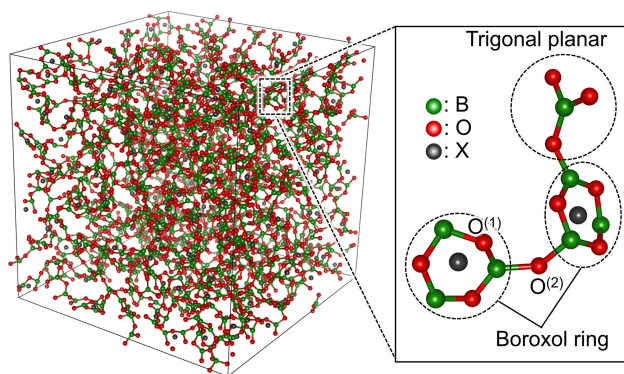


Fig. 1. Initial atomic configuration of B_2O_3 glass.

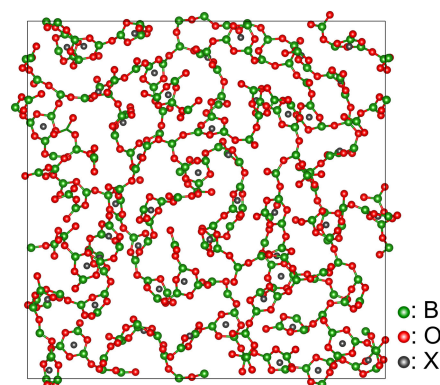


Fig. 3. Atomic configuration of B_2O_3 glass obtained by RMC modeling (7-Å-thick slice).

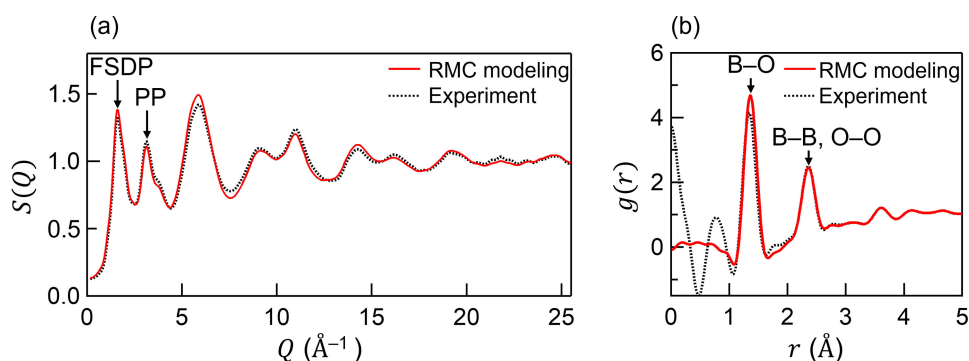


Fig. 2. (a) Total structure factor $S(Q)$ and (b) pair distribution function $g(r)$ obtained by RMC modeling together with the experimental high-energy XRD data for B_2O_3 glass.

RMC model using the R.I.N.G.S. code.^{37,38)} The surface cavity analysis of the RMC model of B_2O_3 glass was conducted using the pyMolDyn code³⁹⁾ with a cutoff distance $r_c = 2.5$ Å. Persistent homology analyses⁴⁰⁾ were performed to derive the B/O-centric one-dimensional persistence diagram using the HomCloud Package.^{40,41)} For the analyses of the ring size distribution, cavity, and persistent homology, the dummy X atoms were removed.

3. Results

Figure 2(a) shows the structure factors $S(Q)$ of B_2O_3 glass obtained from the RMC calculations [$S^{\text{RMC}}(Q)$] and the XRD measurements [$S^{\text{exp}}(Q)$]. Excellent agreement between calculation and experimental results is confirmed. In particular, the first sharp diffraction peak (FSDP) observed at $Q \sim 2$ Å⁻¹ and the PP observed at $Q \sim 3.5$ Å⁻¹ in the $S^{\text{exp}}(Q)$ are well reproduced by the RMC modeling in terms of both peak position and height. The R -factor reached a value of 11.3 %, which indicates that the three-dimensional structure constructed by RMC modeling accurately reflects the experimental data. Note that the PP is clearly observed in XRD data unlike in the case of SiO_2 glass, because the atomic number of B is smaller than that of O; consequently, the positive contribution from the O–O partial $S(Q)$ is larger than the negative contribution from the B–O partial $S(Q)$ at the position of the PP.^{19,20)} The agreement with the experimental XRD data demonstrates

the overall structural consistency, while the fraction of boroxol rings is examined in detail below.

Figure 2(b) shows the pair distribution functions $g(r)$ of B_2O_3 glass derived by the Fourier transforms of $S^{\text{RMC}}(Q)$ and $S^{\text{exp}}(Q)$, denoted as $g^{\text{RMC}}(r)$ and $g^{\text{exp}}(r)$, respectively. A Lorch modification function was applied to the data up to $Q_{\text{max}} = 25$ Å⁻¹. Here, we can confirm a very good agreement between the $g^{\text{RMC}}(r)$ and $g^{\text{exp}}(r)$. The peaks observed at 1.35 and 2.36 Å correspond to the B–O bonds and B–B/O–O correlations, respectively. Their positions are in accordance with the previously reported values of 1.35–1.37 and 2.36–2.38 Å.^{1,7,31)}

Figure 3 shows a slice of the atomic configuration of B_2O_3 glass obtained by RMC modeling. It is confirmed that a number of boroxol rings maintain their hexagonal shapes around the dummy X atoms. **Figure 4** shows the partial pair distribution functions, $g_{ij}(r)$ of B_2O_3 glass derived from the RMC model. The peak positions of B–O, B–B, and O–O correlations in $g_{ij}(r)$ are in agreement with the interatomic distances in B_2O_3 glass reported in a previous study.¹⁾ Note that the O–X, and B–X peaks are observed at around 1.35 Å, which is consistent with the B–O distance, demonstrating that the symmetric shape of the boroxol rings is maintained during the RMC modeling.

The results of the coordination number analysis are summarized in **Table 1**. The B–O coordination number of 2.99, which is close to 3.00, indicating that the basic

structural units of B₂O₃ glass, i.e., boroxol rings and the trigonal planar units, are properly formed in the model. Furthermore, the X–B and X–O coordination numbers are both 3.00, demonstrating that the shape of the 320 boroxol rings, which corresponds to $f = 80\%$, has been maintained without significant distortion.

The bond angle distributions $B(\theta)/\sin\theta$ of B₂O₃ glass are shown in Fig. 5. The O–B–O and B–O–B bond angle distributions exhibit peaks at approximately 120° in Figs. 5(a) and 5(b). These peaks primarily originate from the O–B–O and B–O–B bond angle distributions within the boroxol rings, as evidenced by the these distributions

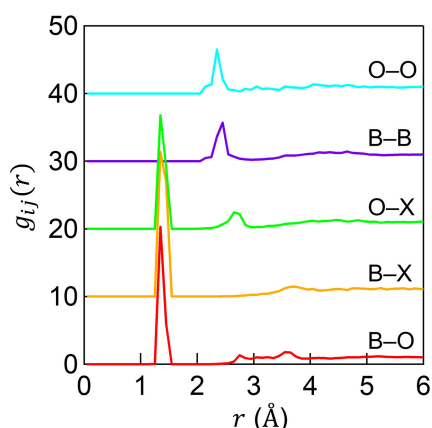


Fig. 4. Partial pair distribution functions, $g_{ij}(r)$ obtained from the RMC model for B₂O₃ glass.

Table 1. Coordination numbers in B₂O₃ glass obtained from the RMC model

Atomic pair	Coordination number
B–O	2.99
X–B	3.00
X–O	3.00

calculated from bond angles exclusively in the boroxol rings (dashed curves), which produce a sharp distribution. This feature indicates that the symmetric shape of the boroxol rings is preserved during the RMC modeling. This symmetric hexagonal shape is further supported by the peaks at 60° in the B–B–B and O–O–O distributions [Figs. 5(c) and 5(d)], and at 30 and 90° in the O–B–B and O–O–B distributions [Figs. 5(e) and 5(f)]. Moreover, as shown in Fig. S1 in Supporting Information, the B–X–O, B–O–X, and X–B–O distributions exhibit peaks at around 60°, the O–X–O and B–X–B distributions at around 120°, and the X–B–B distribution at around 30°. Additionally, the $B(\theta)/\sin\theta$ value increases as θ approaches 180° in the X–B–O distribution. These features correspond well to the symmetric shape of the hexagonal boroxol rings.

The results of the coordination numbers and bond angle distributions together with the excellent agreement between $S^{\text{RMC}}(Q)$ and $S^{\text{exp}}(Q)$ described above consistently demonstrate that the structure of B₂O₃ glass with a large number of boroxol rings has been successfully reproduced, highlighting the capability of the present method to construct a realistic structural model of borate glass. Importantly, this large fraction of boroxol rings is achieved without compromising the agreement with the experimental XRD data shown in Fig. 2.

4. Discussion

Figure 6(a) shows the primitive⁴²⁾ (B–O)_n ring size distribution obtained from the RMC model of B₂O₃ glass. As can be seen in the figure, it has a large fraction of threefold rings, indicating that the boroxol rings are the dominant structural unit in the glass. The total number of boroxol rings incorporating 972 B atoms is 324. Therefore, the fraction f is estimated to be $972/1200 = 0.81$. In addition, as clearly shown in the inset of Fig. 6(a), a certain fraction of the larger rings ($n > 3$) is present, which is attributed to larger rings formed by the linkage of multiple

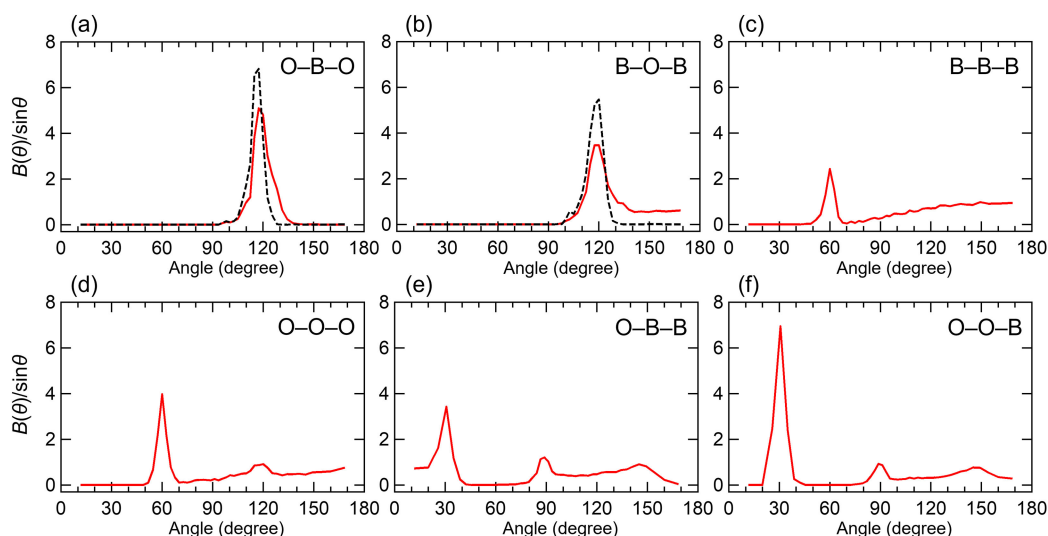


Fig. 5. Bond angle distributions of (a) O–B–O, (b) B–O–B, (c) B–B–B, (d) O–O–O, (e) O–B–B, and (f) O–O–B obtained from the RMC model for B₂O₃ glass. Dashed curves in (a) and (b) indicate the bond angle distributions within the boroxol rings.

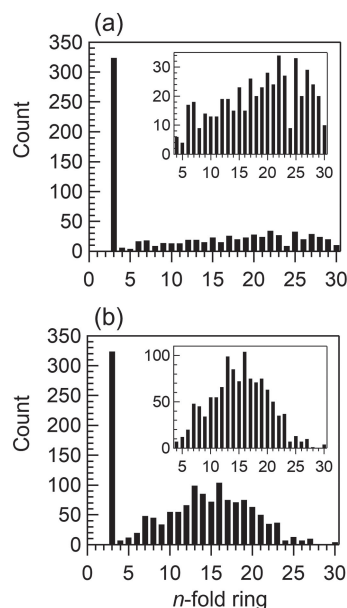


Fig. 6. $(\text{B}-\text{O})_n$ ring size distributions of the RMC model for B_2O_3 glass calculated using the (a) primitive and (b) King criteria.

boroxol rings via $\text{O}^{(2)}$ atoms. Figure 6(b) shows the ring size distribution calculated on the basis of King's criterion.⁴³⁾ It exhibits 324 boroxol rings, as observed in the primitive ring size distribution. However, compared with the primitive rings, it shows a clearer ring size distribution ranging from 4- to 23-fold [inset of Fig. 6(b)]. The difference arose from different algorithms in the two criteria; the primitive ring size distribution enumerates all the shortest closed paths along with B–O bonds within a maximum search depth, exhibiting a broader distribution including larger rings ($n > 24$). In contrast, King's criterion enables the finding of a combination of boroxol (threefold) rings and other rings, which cannot be detected by the primitive ring criterion, because it cannot detect a decomposable (nonprimitive) ring. [see Refs. 37) and 38) for details of ring size statistical analysis]. Indeed, the presence of the larger rings, excluding the boroxol rings, demonstrates the formation of a topologically disordered network, which is a characteristic of glasses.^{44,45)} Nevertheless, the B_2O_3 glass is exceptionally topologically ordered compared with typical glasses such as SiO_2 glass,^{46,47)} owing to the dominant fraction of boroxol rings. Notably, this coexistence is not imposed by explicit constraints on ring sizes in the RMC modeling, but instead emerges naturally from the diffraction-based structural refinement.

Figure 7 shows the persistence diagram obtained from the RMC model for B_2O_3 glass. We can observe a distinct vertical profile along with the death axis at the birth $b \sim 0.5 \text{ \AA}^2$, corresponding to half of the B–O bond. Region I (highlighted in blue) around $b \sim 0.5 \text{ \AA}^2$ and within $1.4 \text{ \AA}^2 < \text{death } (d) < 1.9 \text{ \AA}^2$ corresponds to the birth and death of boroxol rings. This prominent profile is a signature of the topologically ordered feature of B_2O_3 glass, as mentioned above. On the other hand, region II (high-

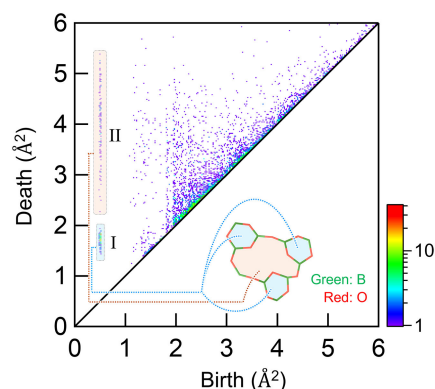


Fig. 7. Persistence diagram of the RMC model for B_2O_3 glass.

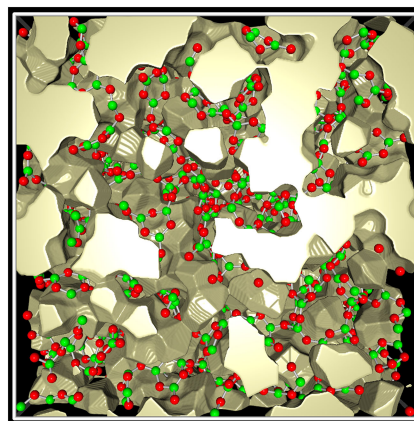


Fig. 8. Visualization of surface-based cavities in the RMC model for B_2O_3 glass. In the image, green and red circles represent B and O atoms, respectively. Cavities are highlighted in gold.

lighted in red) around $b = 0.5 \text{ \AA}^2$ and within $2.2 \text{ \AA}^2 < d < 5.5 \text{ \AA}^2$ corresponds to the profiles originating from larger rings with various sizes, which are observed in the persistence diagrams of SiO_2 glass.^{32,33,48)}

The surface-based cavities of B_2O_3 glass are visualized in Fig. 8. The cavity volume ratio was found to be 34.2 % (12825 \AA^3 of the cell volume of 37500 \AA^3), which is comparable to that of SiO_2 glass.³³⁾ As mentioned in Introduction, the incorporation of other oxides into the structure of B_2O_3 glass gives rise to various physicochemical properties, because such oxides are considered to disrupt the B–O network by occupying the cavity regions associated with the increase in density. Therefore, the information of the cavity obtained in this study should be useful for understanding the origin of various properties in borate glasses induced by the addition of network-modifying oxides. In addition, since the cavities are generally compressed under high pressure, such information may also provide valuable insights into the structural evolution of B_2O_3 glass under compression, which remains an active area to be explored.^{49–53)} Overall, our model provides a reliable basis for further atomistic discussions of its structural and physicochemical properties in B_2O_3 and borate glasses.

5. Conclusion

Using RMC modeling based on high-energy XRD data, we have derived a structural model for B₂O₃ glass, although maintaining a large fraction of boroxol rings has long been considered difficult. The structural model was successfully reproduced by introducing dummy X atoms to stabilize the boroxol rings. The structure factor obtained by the RMC calculation showed excellent agreement with the XRD data. Analysis of the obtained structural model confirmed that a large fraction of symmetric boroxol rings (~80 %) was well reproduced, as evidenced by the coordination number, bond angle distribution, and ring size distribution. In particular, the ring size distribution and persistence diagram revealed a large number of three-membered rings corresponding to the boroxol rings, with only a minor fraction of larger rings, highlighting the exceptionally high topological order of the B₂O₃ glass. Furthermore, cavity analysis based on the structural model was performed, and its fraction was found to be 34.2 %. Our approach can be extended to B₂O₃-based glasses containing various network-modifying oxides and to studies of structural evolution under high pressure, which will provide a firm basis for understanding the physicochemical and structural characteristics of borate glasses at the atomic level.

Acknowledgment This work was partially supported by JSPS Grants-in-Aid for Transformative Research Areas (A) “Hyper-Ordered Structures Science” (Grant Numbers 20H05878, 20H05881, and 20H05884) and Scientific Research (A) (25H00606). The synchrotron radiation experiments were carried out with the approval of the Japan Synchrotron Radiation Research Institute (JASRI) (Proposal Numbers 2008A1377 and 2020A1108).

References

- 1) O. L. G. Alderman, N. S. Tagiara, I. Slagle, R. M. Gabrielson, P. Boggs, M. Wagner, A. Rossini, S. John, L. Rocha, R. M. Wilson, H. Hawbaker, S. W. Martin, A. C. Hannon, E. I. Kamitsos and S. A. Feller, *Rep. Prog. Phys.* **88**, 076501 (2025).
- 2) G. E. Jellison, Jr., L. W. Panek, P. J. Bray and G. B. Rouse, Jr., *J. Chem. Phys.* **66**, 802 (1977).
- 3) C. Joo, U. Werner-Zwanziger and J. W. Zwanziger, *J. Non-Cryst. Solids* **261**, 282 (2000).
- 4) S. Kroeker and J. F. Stebbins, *Inorg. Chem.* **40**, 6239 (2001).
- 5) S. J. Gravina, P. J. Bray and G. L. Petersen, *J. Non-Cryst. Solids* **123**, 165 (1990).
- 6) J. Sakowski and G. Herms, *J. Non-Cryst. Solids* **293–295**, 304 (2001).
- 7) A. Hanon, D. I. Grimley, R. A. Hulme, A. C. Wright and R. N. Sinclair, *J. Non-Cryst. Solids* **177**, 299 (1994).
- 8) T. F. Soules, *J. Chem. Phys.* **73**, 4032 (1980).
- 9) M. Amini, S. K. Mitra and R. W. Hockney, *J. Phys. C Solid State* **14**, 3689 (1981).
- 10) A. Takada, C. R. A. Catlow and G. D. Price, *J. Phys.-Condens. Mat.* **7**, 8693 (1995).
- 11) P. Umari and A. Pasquarello, *Phys. Rev. Lett.* **95**, 137401 (2005).
- 12) G. Ferlat, T. Charpentier, A. P. Seitsonen, A. Takada, M. Lazzeri, L. Cormier, G. Calas and F. Mauri, *Phys. Rev. Lett.* **101**, 065504 (2008).
- 13) S. S. Sørensen, H. Johra, J. C. Mauro, M. Bauchy and M. M. Smedskjaer, *Phys. Rev. Mater.* **3**, 075601 (2019).
- 14) A. Baroni, F. Pacaud, M. Salanne, M. Micoulaut, J.-M. Delaye, A. Zeidler, P. S. Salmon and G. Ferlat, *J. Chem. Phys.* **151**, 224508 (2019).
- 15) D. Meher, N. V. S. Avula and S. Balasubramanian, *J. Chem. Phys.* **162**, 044503 (2025).
- 16) L. A. Avakyan, A. V. Skidanenko, Y. A. Vakulenko, E. A. Tretyakov, G. Y. Shakhgulyan, V. N. Sigaev and L. A. Bugaev, *J. Struct. Chem.* **66**, 165 (2025).
- 17) S. Urata and F. Lodesani, *Materialia* **42**, 102474 (2025).
- 18) J. Swenson and L. Börjesson, *Phys. Rev. B* **55**, 11138 (1997).
- 19) K. Suzuya, Y. Yoneda, S. Kohara and N. Umesaki, *Phys. Chem. Glasses* **41**, 282 (2000).
- 20) H. Ohno, S. Kohara, N. Umesaki and K. Suzuya, *J. Non-Cryst. Solids* **293–295**, 125 (2001).
- 21) M. Fábán, E. Sváb, T. Proffen and E. Veress, *J. Non-Cryst. Solids* **356**, 441 (2010).
- 22) H. Doweidar, *J. Mater. Sci.* **25**, 253 (1990).
- 23) N. M. Bobkova, *Glass Phys. Chem.* **29**, 501 (2003).
- 24) M. Bengisu, *J. Mater. Sci.* **51**, 2199 (2016).
- 25) S. Sasaki and A. Masuno, *J. Ceram. Soc. Jpn.* **130**, 60 (2022).
- 26) Y. Fujimoto, T. Yanagida, M. Koshimizu and K. Asai, *J. Ceram. Soc. Jpn.* **125**, 728 (2017).
- 27) I. Avramov, Ts. Vassilev and I. Penkov, *J. Non-Cryst. Solids* **351**, 472 (2005).
- 28) O. L. G. Alderman, *J. Chem. Phys.* **162**, 054502 (2025).
- 29) R. L. McGreevy and L. Pusztai, *Mol. Simulat.* **1**, 359 (1988).
- 30) A. K. Soper, *Chem. Phys.* **202**, 295 (1996).
- 31) A. K. Soper, *J. Phys.-Condens. Mat.* **23**, 365402 (2011).
- 32) Y. Onodera, S. Kohara, P. S. Salmon, A. Hirata, N. Nishiyama, S. Kitani, A. Zeidler, M. Shiga, A. Masuno, H. Inoue, S. Tahara, A. Polidori, H. E. Fischer, T. Mori, S. Kojima, H. Kawaji, A. I. Kolesnikov, M. B. Stone, M. G. Tucker, M. T. McDonnell, A. C. Hannon, Y. Hiraoka, I. Obayashi, T. Nakamura, J. Akola, Y. Fujii, K. Ohara, T. Taniguchi and O. Sakata, *NPG Asia Mater.* **12**, 85 (2020).
- 33) Y. Onodera, *J. Ceram. Soc. Jpn.* **130**, 627 (2022).
- 34) R. Toyoda, K. Usui, T. Hirota, K. Kimura, Y. Onodera, M. R. Cicconi, R. Belli, M. Brehl, J. Lubauer, U. Lohbauer, H. Tajiri, K. Ikeda, T. Hayakawa, D. de Ligny, S. Kohara and K. Hayashi, *J. Non-Cryst. Solids* **616**, 122472 (2023).
- 35) K. Ohara, Y. Onodera, M. Murakami and S. Kohara, *J. Phys.-Condens. Mat.* **33**, 383001 (2021).
- 36) O. Gereben, P. Jónvári, L. Temleitner and L. Pusztai, *J. Optoelectron. Adv. M.* **9**, 3021 (2007).
- 37) S. Roux and P. Jund, *Comput. Mater. Sci.* **49**, 79 (2010).
- 38) S. Roux and P. Jund, *Comput. Mater. Sci.* **50**, 1217 (2011).
- 39) I. Meyer, F. Rhiem, F. Beule, D. Knodt, J. Heinen and R. O. Jones, *J. Comput. Chem.* **38**, 389 (2017).
- 40) T. Nakamura, Y. Hiraoka, A. Hirata, E. G. Escobar and Y. Nishiura, *Nanotechnology* **26**, 304001 (2015).

- 41) I. Obayashi, T. Nakamura and Y. Hiraoka, *J. Phys. Soc. Jpn.* **91**, 091013 (2022).
- 42) C. S. Mariani and L. W. Hobbs, *J. Non-Cryst. Solids* **124**, 242 (1990).
- 43) S. V. King, *Nature* **213**, 1112 (1967).
- 44) A. R. Cooper, *Phys. Chem. Glasses* **19**, 60 (1978).
- 45) P. K. Gupta, *J. Am. Ceram. Soc.* **76**, 1088 (1993).
- 46) S. Kohara, M. Shiga, Y. Onodera, H. Masai, A. Hirata, M. Murakami, T. Morishita, K. Kimura and K. Hayashi, *Sci. Rep.-UK* **11**, 22180 (2021).
- 47) S. Kohara, S. Sato, M. Shiga, Y. Onodera, H. Masai, T. Wakihara, A. Masuno, A. Hirata, N. Kitamura, Y. Idemoto, K. Kimura and K. Hayashi, *J. Ceram. Soc. Jpn.* **132**, 653 (2024).
- 48) Y. Hiraoka, T. Nakamura, A. Hirata, E. G. Escobar, K. Matsue and Y. Nishiura, *P. Natl. Acad. Sci. USA* **113**, 7035 (2016).
- 49) S. K. Lee, P. J. Eng, H.-K. Mao, Y. Meng, M. Newville, M. Y. Hu and J. Shu, *Nat. Mater.* **4**, 851 (2005).
- 50) V. V. Brazhkin, Y. Katayama, K. Trachenko, O. B. Tsiok, A. G. Lyapin, E. Artacho, M. Dove, G. Ferlat, Y. Inamura and H. Saitoh, *Phys. Rev. Lett.* **101**, 035702 (2008).
- 51) A. Zeidler, K. Wezka, D. A. J. Whittaker, P. S. Salmon, A. Baroni, S. Klotz, H. E. Fischer, M. C. Wilding, C. L. Bull, M. G. Tucker, M. Salanne, G. Ferlat and M. Micoulaut, *Phys. Rev. B* **90**, 024206 (2014).
- 52) H. Kuang, Y. Pan and J. S. Tse, *J. Phys. Chem. C* **128**, 3543 (2024).
- 53) G. Carini, Jr., G. Carini, G. D'Angelo, M. Federico and V. Romano, *J. Non-Cryst. Solids* **492**, 102 (2018).